Radiative properties of matter based on quantum statistical method

Rukhsana Kouser[1], G Tasneem[1], Muhammad Saleem Shahzad[1], S Sardar[1,2,†], Amjad Ali[1], M H Nasim[1], and M Salahuddin[1]

[1] *Department of Physics and Applied Mathematics, Pakistan Institute of Engineering and Applied Sciences, Nilore, Islamabad* 45650, *Pakistan*

[2] *Hefei National Laboratory for Physical Sciences at Microscale and Department of Modern Physics, University of Science and Technology of China, Hefei* 230026, *China*

(Received 18 February 2017; revised manuscript received 31 March 2017; published online 17 May 2017)

We present the preliminary results of our code OPAQS (opacity calculation using quantum statistical model) that is based on the self consistent Hartree–Fock–Slater model for the average atom. The code is capable of performing robust calculations of average charge state, frequency-dependent and mean opacities. The accuracy of the atomic model is verified by comparing the calculations of average charge state with various published results. The monochromatic opacities for iron computed at different sets of temperatures and densities are compared with LEDCOP. The Rosseland and Planck opacities for iron and aluminum are validated with some state-of-the-art codes. The results are in good agreement with the published data.

Keywords: self-consistent average atom model, average ionization state, Rosseland opacity, Planck opacity

PACS: 52.25.Os, 32.30.–r, 31.15.xr **DOI:** 10.1088/1674-1056/26/7/075201

1. Introduction

Radiative properties provide us with insight about the behavior of the matter during its interaction with a radiation field. In astrophysics and environmental science, the more specific term used for referring to radiative properties is opacity: a measure of the resistance of matter to the transmission of radiation. There are various absorption and scattering mechanisms that impede the transmission and make the material opaque to radiation, such as photo-excitation, photo-ionization, inverse bremsstrahlung, and Thomson scattering. The experimental determination of opacity relies on transmission/absorption and emission spectroscopic techniques.[1–3] However, there are many practical situations in which measurements cannot be achieved in laboratory experiments, hence theoretical predictions of opacities are inevitable.[4]

Fast and accurate calculations of radiative properties are crucial for performing radiation hydrodynamic simulations and spectroscopic diagnostics in diverse research areas, such as stellar physics, inertial and magnetic confinement fusions. While modeling such problems, average charge state and photon absorption coefficient data must be available in the wide range of density and temperature. In this regard, extensive calculations need to be performed.[5–7] A few years back, these calculations were limited because of the limited capacity of the computers, so approximate atomic physics models were developed.[8–13] Significant advances in computational techniques have taken place, so with refined numerical methods and improved computational techniques now detailed and more complex approaches to opacity calculations are possible to implement.[14–17] However, due to the fast computational speed, the average models are still used widely where detailed calculations can be compromised.[1]

In thermodynamic equilibrium, free electrons follow the Maxwell–Boltzmann distribution, whereas the energy density distribution of photons is given by the Planck distribution. Our model is based on local thermodynamic equilibrium (LTE), which implies that at any particular instant, photon and electron distributions are in equilibrium with each other. From a computational point of view, LTE simplifies the calculations because instead of solving detailed rate equations, the atomic level populations can be found by Saha and Boltzmann equations, without requiring any fundamental cross section calculations.[18]

Many computational and experimental efforts are going on in parallel for achieving reliable opacities data.[1,7,19–32] It includes a large list, but here we are giving a short introduction to some of the sources, which we have used for comparison of our results. The opacity project (OP)[33] and opacity project at Livermore (OPAL)[34] have been the early sources of opacity data for astrophysicists since the nineties, and are still used extensively for modeling various problems in stellar physics.[1] OP is an online database in which atomic data is calculated using the R-matrix method, utilizing the close-coupling approximation.[33] OPAL code calculates the solution of the Schrödinger wave equation by applying relativistic analytical potential, and level populations are found by the minimization of the system's free energy.[34] SCO-RCG is a hybrid code and combines detailed level and statistical approaches.[35] The most recent and widely tested code in the

†Corresponding author. E-mail: sardar@mail.ustc.edu.cn

© 2017 Chinese Physical Society and IOP Publishing Ltd

field of stellar physics is OPAS, which is based on LTE and performs calculations by combining detailed configuration and level accounting methods.[36] STA code interpolates smoothly between detailed configuration accounting and average-atom approach.[37] CASSANDRA code utilizes a detailed configuration method for obtaining atomic data and an *ab-initio* method for the computation of atomic physics, employing the Dirac–Hartree–Slater approximation.[38] CORONA code obtains atomic data from Perrot's screened hydrogenic model, and average atom model in the Thomas–Fermi approach is used for average ionization.[39] LEDCOP code uses the relativistic self-consistent Hartree–Fock method, and ionic populations are calculated by using the Saha equation.[40] THERMOS code makes use of relativistic analytical potential in solving the Schrödinger equation, and calculates occupation numbers using an average atom model.[7]

The model presented in this paper is based on the average atom approximation. At high temperature ($T > 10$ eV), this approximation is widely used to describe the state of matter.[41] The self-consistent potential in the average atom model is calculated for an ion with average occupation numbers of energy levels, along with the free electrons in the charge-neutral spherical cell. The cross sections for radiative properties are used in the non-relativistic limits. The atomic model is mainly adopted from Ref. [7] with the exception that we have implemented the numerical scheme of Refs. [42] and [43] for the solution of the Schrödinger equation.

This paper provides the sketch of a near-future research program as much as reporting on the first steps. Some results of our model have been reported previously[44,45] in which calculations were validated with some of the advanced codes, and the results were also tested in radiation hydrodynamic code MULTI-2D.[46] In what follows, Section 2 presents the mathematical details of the model. The numerical scheme is described in Section 3. The results are compared with the published results[47] in Section 4. Finally, Section 5 presents our conclusions.

2. Mathematical modeling

2.1. Calculation of energy levels by using self-consistent potential

In our calculations, it is assumed that a well-defined average atom can show the average behavior of all the atoms and ions at that temperature and density. This average atom is a fictitious atom with non-integral occupation numbers. It occupies a spherical cell in which a nucleus is present at the center and electrons are distributed around it following a radial distribution. The volume of the cell is defined by the mean volume per atom as

$$\frac{4}{3}\pi(r_{\rm o}a_{\rm o})^3 = \frac{A}{\rho_{\rm m}N_{\rm A}}, \tag{1}$$

where A is the atomic mass, $\rho_{\rm m}$ is the mass density, $a_{\rm o}$ is the Bohr radius, and $N_{\rm A}$ is Avogadro's number. Hence the average radius $r_{\rm o}$ (in atomic units) is

$$r_{\rm o} = 1.388\left(\frac{A}{\rho_{\rm m}}\right)^{1/3}. \tag{2}$$

After defining the atomic sphere, we solve the system of Hartree–Fock–Slater (HFS) equations for the self-consistent potential and wave functions. These calculations need the intra-atomic potential and distribution of electrons within the cell. We have taken these values from the Thomas–Fermi model[7] as the first guess. The HFS equations are given by

$$\left(-\frac{1}{2}\Delta - V(r)\right)\psi_{\rm a}(r) = E_{nl}\psi_{\rm a}(r), \tag{3}$$

where E_{nl} are energy eigenvalues and $V(r)$ is the HFS potential expressed as

$$V(r) = \frac{Z}{r} - \int \frac{\rho(r')}{|r-r'|}{\rm d}r' + V_{\rm ex}, \tag{4}$$

with ρ being the radial distribution of electrons within the cell and $V_{\rm ex}$ the exchange potential given by[5,7]

$$V_{\rm ex}(r) = \frac{\pi\rho(r)}{T}\left[1 + \frac{6\rho(r)}{T^{3/2}} + \frac{\pi^4\rho^2(r)}{3T^3}\right]^{-1/3}. \tag{5}$$

For the above equations to be solvable, the wave function must be separable. We have taken wave function $\psi_{\rm a}(r)$ of the form

$$\psi_{\rm a}(r) = \psi_{nlm}(r) = \frac{1}{r}R_{nl}(r)Y_{lm}(\theta,\phi),$$

where $Y_{lm}(\theta,\phi)$ is the spherical harmonics, $R_{nl}(r)$ are the radial wave functions, and nlm is the set of quantum numbers defining the state of electron. The numerical procedure for calculation of E_{nl} and $R_{nl}(r)$ is taken from Ref. [42] that solves the Schrödinger equation by piecewise exact power series expansion of radial wave functions.[43] These series are then summed up with prescribed accuracy and the solution is obtained.

The radial electron density $\rho(r)$ is taken as a sum of the bound and free electrons

$$\rho(r) = \rho_{\rm b}(r) + \rho_{\rm f}(r). \tag{6}$$

The contribution of the bound states, $\rho_{\rm b}(r)$, is calculated by using the radial wave functions as

$$\rho_{\rm b}(r) = \frac{1}{4\pi r^2}\sum P_{nl}R_{nl}^2(r),$$
$$P_{nl} = \frac{2(2l+1)}{1+\exp\left(\dfrac{E_{nl}-\mu}{T}\right)}, \tag{7}$$

where T is the temperature of plasma and μ is the chemical potential (both in atomic units).

The free electrons density $\rho_{\rm f}(r)$ is calculated using the Thomas–Fermi model[7]

$$\rho_{\rm f}(r) = \frac{2}{(2\pi)^3}\int_{p^2/2-V(r)>E_0} \frac{4\pi p^2 {\rm d}p}{1+\exp\left(\dfrac{p^2-V(r)-\mu}{T}\right)}, \quad (8)$$

where E_0 is the effective boundary of continuum, and is determined from the thermodynamic consistency condition. We have not included the effect of continuum lowering explicitly as a correction term in the equation of the energy levels, as this effect is indirectly encountered through the effective boundary of the continuum.[12] For high temperature, a good approximation for the free electron density is $\rho_{\rm f}(r) = \rho_{\rm e}$, where $\rho_{\rm e}$ is assumed to be equal to the electron density at the atomic shell boundary

$$\rho_{\rm e} = \frac{\sqrt{2}T^{3/2}}{\pi^2}\int_{y_0}^{\infty} \frac{y^{1/2}{\rm d}y}{1+\exp(y-x)}, \quad (9)$$

where

$$y_0 = \max\left(\frac{V(r_0)+E_0}{T}, 0\right), \quad (10)$$

$$x = \frac{V(r_0)+\mu}{T}, \quad V(r_0) = V_{\rm ex}(r_0). \quad (11)$$

Finally, the mean charge $Z_{\rm o}$ can be calculated by

$$Z_{\rm o} = \frac{4}{3}\pi {r_{\rm o}}^3 \rho_{\rm e}. \quad (12)$$

Equations (3)–(12) are solved in self-consistent manner.

2.2. Calculation of frequency-dependent opacity

Once the average charge state, energy levels, and occupation numbers have been determined, the total frequency-dependent opacity $k(\nu)$ is calculated as the sum of photo-excitation (bound–bound), photo-ionization (bound–free), inverse bremsstrahlung (free–free), and scattering processes as[18]

$$k(\nu) = [k^{\rm bb}(\nu)+k^{\rm bf}(\nu)+k^{\rm ff}(\nu)](1-{\rm e}^{-h\nu/T})+k^{\rm scat}, \quad (13)$$

where k denotes the cross section of the above-mentioned processes. The sum in the square brackets signifies the total cross section of the three frequency-dependent absorption processes, i.e., bound–bound, bound–free, and free–free transitions, respectively, and is corrected for the induced emission (the term in parenthesis). The scattering is taken in the classical domain where it is independent of frequency. All the coefficients are calculated using the average atom model[13] and described in the following sections.

2.2.1. Photo-excitation coefficient

Photo-excitation coefficient $k^{\rm bb}$ as a function of photon energy can be calculated as[48]

$$k^{\rm bb}_{kk'}(\nu) = \frac{6.602\times10^4}{A} f_{kk'}\Psi_{kk'}(\nu), \quad (14)$$

where $f_{kk'}$ is the oscillator strength corresponding to the transition between an initial state $k=(n,l)$ and a final stage $k'=(n',l')$ and given by

$$f_{k,k'} = \frac{2}{3}(E_{k'}-E_k)\frac{l+l'+1}{2(2l+1)}R^2_{k,k'}, \quad l'=l\pm1, \quad (15)$$

where $R^2_{k,k'}$ are the radial matrix elements between levels k and k', and computed by the relation

$$R_{k,k'} = \int_0^{r_0} R_k(r) r R_{k'}(r) {\rm d}r. \quad (16)$$

The integration is carried out by using the trapezoidal rule. The method of finding $R_k(r)$ has already been described in the previous section.

The $\Psi_{kk'}(\nu)$ in Eq. (15) is the line broadening profile. The best choice of the line profile that incorporates the behavior of all broadenings is the Voigt profile, which is the convolution of Lorentzian and Gaussian profiles. In our model, the Voigt profile gathers natural, Doppler, fine structure, Stark, and collisional broadenings to find out line shape function $\Psi_{kk'}(\nu)$ as

$$\Psi_{kk'}(\nu) = \frac{1}{\sqrt{\pi}} V\left(\frac{h\nu-(|E_k-E_{k'}|)}{\gamma^{\rm G}_{kk'}}, \frac{\gamma^{\rm L}_{kk'}}{\gamma^{\rm G}_{kk'}}\right), \quad (17)$$

where V is the Voigt function, $\gamma^{\rm G}_{kk'} = \sqrt{(\gamma^{\rm d}_{kk'})^2+(\gamma^{s}_{k'})^2}$ is the overall width of broadenings with Gaussian profile, and $\gamma^{\rm L}_{kk'} = \gamma^{\rm n}_{kk'}+\gamma^{c}_{k'}+\gamma^{\rm f}_{kk'}$ is the sum of broadenings having the Lorentzian profile.[49]

The standard formulas are used for natural $\gamma^{\rm n}$ and Doppler width $\gamma^{\rm d}$,[48] which are given by

$$\gamma^{\rm n}_{kk'} = 4.75\times10^{-6}(E_k-E_{k'})^2, \quad (18)$$

$$\gamma^{\rm d}_{kk'} = 1.036\times10^{-3}\,|E_k-E_{k'}|\,(T/A)^{1/2}. \quad (19)$$

Hydrogen-like approximation is used for both the fine structure width $\gamma^{\rm f}$[50] and Stark broadening γ^{s}, which are expressed as

$$\gamma^{\rm f}_{kk'} = \left(\frac{13.6\times10^{-3}}{137^2}\right)\left(\frac{Z_n^4}{n^3l(l+1)}+\frac{Z_{n'}^4}{n'^3l'(l'+1)}\right), \quad (20)$$

$$\gamma^{s}_{k'} = \left(\frac{(1.25a_{\rm o}^2)(27.21\times10^{-3}Z_{\rm o})}{Z_{n'}r_{\rm o}^2}\right)\left(3n'^2-l'(l'+1)\right). \quad (21)$$

Electron collisional broadening γ^{c} is obtained by using the screened nuclear charge instead of the effective principal quantum numbers, and calculated as[48]

$$\gamma^{c}_{k'} = 1.268\times10^{-3}\frac{Z_{\rm o}\rho_{\rm m}}{AT^{1/2}}\left(\frac{n'}{Z_{n'}}\right)^2 \times\left(5n'^2+1-3l'(l'+1)\right). \quad (22)$$

All broadening mechanisms are not equally likely, the dominance of any particular phenomenon takes place depending upon the plasma conditions.

2.2.2. Photo-ionization coefficient

The photo-ionization cross section is taken in the nonrelativistic approximation, calculated as

$$k^{\rm bf}(\nu) = \frac{3\pi}{4}c^3\sigma_{\rm o}\sum P_k \frac{2\pi\nu}{1+\exp\left(\dfrac{E-\mu}{T}\right)}\sum f_{k,El'}, \quad (23)$$

where $\sigma_{\rm o}$ is the Thomson cross section and $f_{k,El'}$ is the oscillator strength for the bound-free transition given by[5]

$$f_{k,El'} = \begin{cases} \dfrac{l+l'+1}{3(2l+1)}R^2_{k,El'}, & l' = l\pm 1, \\ 0, & l' \neq l\pm 1, \end{cases} \quad (24)$$

with $R_{k,El'}$ being the continuum wave functions. We have computed $R_{k,El'}$ using the semiclassical approximation for the central field (WKB method). The detail is given in Appendix A. 4 of Ref. [7].

2.2.3. Inverse bremsstrahlung coefficient

For inverse bremsstrahlung coefficient, the results of hydrogen atom are used[48]

$$k^{\rm ff}(\nu) = 2.78\left(\frac{Z_{\rm o}^3\rho_{\rm m}}{A^2T^{1/2}(h\nu)^3}\right)g^{\rm ff}\phi, \quad (25)$$

where $g^{\rm ff}$ is the Gaunt factor and ϕ is the degeneracy correction. The Gaunt factor $g^{\rm ff}$ is given by[48,51]

$$g^{\rm ff} = 1+0.1728\left(\frac{h\nu}{13.6\times 10^{-3}Z_{\rm o}^2}\right)^{1/3}(1+2\frac{T}{h\nu}). \quad (26)$$

The degeneracy factor ϕ is taken as[48,52]

$$\phi = \frac{\pi^{1/2}}{2}\frac{\ln\left(\dfrac{1+\exp(-\mu/T)}{1+\exp[(-\mu-h\nu)/T]}\right)}{F_{1/2}(\mu/T)[1-\exp(-h\nu/T)]}, \quad (27)$$

where $F_{1/2}(\mu/T)$ is the Fermi–Dirac integral of order $1/2$.[7]

2.2.4. Scattering coefficient

At high temperatures, the absorption cross sections for the above three processes fall to very low values, which causes a problem in numerical calculations for Rosseland mean (being the harmonic mean which diverges at very low values). Hence, scattering has to be added as the lower bound in the absorption coefficient to avoid numerical divergence.[2] Our model is currently capable of performing calculations in non relativistic limits only, so we have used Thomson scattering, which is the classical limit of Compton scattering (energy less than electron rest mass energy). It is classified as coherent scattering and given by

$$k^{\rm scat} = 0.4\frac{Z_{\rm o}}{A}. \quad (28)$$

The contributions determined from Eqs. (14), (23), (25), and (28) are substituted in Eq. (13) to obtain the total frequency-dependent opacity (also known as extinction or attenuation coefficient).

2.3. Mean opacities

The radiation hydrodynamic codes require the coupling of the radiation transfer equation (RTE) with the hydrodynamic equations. The frequency-dependent opacity $k(\nu)$ appearing in RTE is a highly nonlinear function of frequency, with sudden jumps owing to the presence of ionization edges and bound–bound resonances. These sharp changes in opacity need to be tactfully handled while performing numerical calculations, as they can cause divergence at particular points. Moreover, $k(\nu)$ calculated on a fine mesh of temperature, density, and frequency points also increases the computational cost of radiation hydrodynamic simulations. The conventional practice to simplify this situation is to replace $k(\nu)$ with the appropriate average. Two widely used types of mean opacities are the Planck and Rosseland opacities, which are calculated by taking the weighted average of $k(\nu)$ over the entire spectrum. The Rosseland mean opacities are of interest in optically thick plasmas, whereas the Planck mean opacities are important for optically thin plasmas. The Planck and Rosseland mean opacities in the photon energy range are defined by[53]

$$k_{\rm P} = \frac{1}{\rho_{\rm m}}\frac{\int_0^\infty {\rm d}\nu U(\nu,T)\,(k(\nu)-k^{\rm scat})}{\int_0^\infty {\rm d}\nu U(\nu,T)}, \quad (29)$$

$$k_{\rm R} = \frac{1}{\rho_{\rm m}}\frac{\int_0^\infty {\rm d}\nu \dfrac{\partial U(\nu,T)}{\partial T}}{\int_0^\infty {\rm d}\nu \dfrac{\partial U(\nu,T)}{\partial T}\dfrac{1}{k(\nu)}}, \quad (30)$$

where $\rho_{\rm m}$ is the mass density and $k(\nu)$ is the extinction coefficient given by Eq. (13), T is the plasma temperature in eV and $U(\nu,T)$ is the Planck function expressed as

$$U(\nu,T) = \frac{2h\nu^3}{c^2}\frac{1}{\exp(h\nu/T)-1}.$$

Note that the Rosseland mean opacity is calculated by taking the harmonic average of the extinction coefficient (absorption + scattering), whereas the Planck mean opacity is obtained by the arithmetic mean of the total absorption coefficient (without scattering). The numerical scheme for the calculation of the mean opacities is adopted from Ref. [54].

3. Numerical implementation

By using the methodology given in the previous section, a computer code OPAQS has been developed for the calculation of the average charge state, monochromatic and mean opacities. A schematic flow diagram of the program is shown in Fig. 1. Computation starts with the guess potential and

radial electron density, which are provided by the Thomas–Fermi model, using the double-sweep method.[7] Next, the Schrödinger wave equation with self-consistent potential is solved numerically using the power series method. The solution of the Schrödinger equation gives the radial wave functions, energy levels, mean occupation numbers, and average ionization. From this information, the absorption coefficients and mean opacities are calculated.

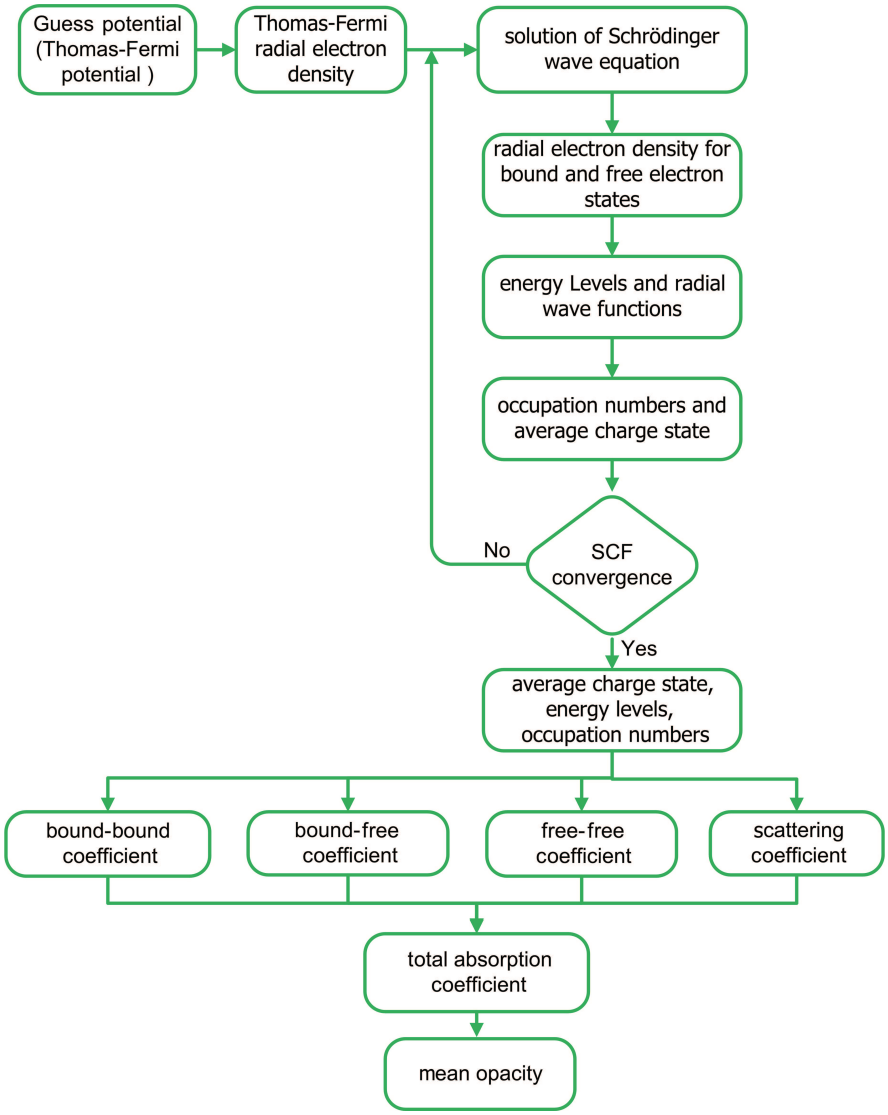


Fig. 1. (color online) Algorithm for OPAQS code.

4. Results and discussion

In order to determine the reliability of a computer code, comparison with available cutting-edge experimental measurements is necessary. In the case of unavailability of experimental data, alternate choice becomes a comparison with state-of-the-art theoretical models and computer codes. As we are intended to show the strengths and weaknesses of our model, so the main purpose of this section is to carry out the validation of the results computed with OPAQS. We have mainly benchmarked the results of OPAQS with LEDCOP, because of its availability and extensive use in research. However, comparison is also made with many other published results, wherever possible. In what follows, we have validated our results of radial wave function, average charge state, frequency-dependent and mean opacities.

The calculations of radial wave functions (R_{nl}) are vital for the calculations of shell occupancies and oscillator strengths. The accuracy of R_{nl} guarantees the accuracy of atomic data (such as energy levels, occupation numbers, and average charge state) and opacity coefficients (bound–bound and bound–free). Figure 2 shows the results of our $R_{nl}(r)$ calculations for aluminium plasma at temperature of 100 eV and density of 0.27 g/cc. The independent variable $(r/r_0)^{1/2}$ is the dimensionless length which is scaled on the radius of the atom cell r_0. It is clear that the radial part of the wave function has a strong dependence on the principle and angular momentum quantum numbers (n and l). The zeros of the function correspond to the nodes of the wave function. The number

of zeros, n_r, follows the relation $n = n_r + l + 1$, hence the 1s curve does not contain any zero, whereas the curves of 2s, 3s and 4s contain one, two, and three zeros, respectively. All the curves vanish at the center and boundary ($r = 0$ and $r = r_0$) of the atom cell, which shows the correct implementation of the boundary conditions. The results are compared with those in Ref. [5] and found to be in excellent agreement.

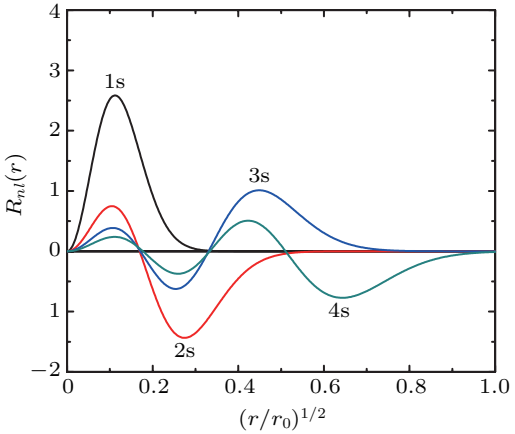


Fig. 2. (color online) The radial wave function $R_{nl}(r)$, $n = 1,2,3,4$, $l = 0$ calculated from the solution of SCF. The calculations are carried out for aluminium at temperature of 100 eV and density of 0.27 g/cc.

The degree of ionization is the most critical parameter in the calculations of atomic properties as it strongly influences many other plasma properties, such as pressure, conductivity, and opacity coefficients. Hence, it is a conventional practice to compare the average charge state (Z_o) as a necessary step while comparing different atomic models. We have validated the results of Z_o with the published results[47] of six extensively used computational tools, including CASSANDRA, CORONA, OPAL, THERMOS, ATMED, and LEDCOP. The calculations are performed for aluminium, germanium, and iron, which are elements of astrophysical and industrial importance. The comparison over a wide range of density and temperature is shown in Tables 1–3. It is clear that in spite of the difference in physical models and computational techniques implemented in different codes, our code shows an excellent agreement for all three elements.

Table 1. Comparison of average charge state for aluminium plasma computed at density of 1 g/cc and temperatures of $T = 500$ eV and $T = 1000$ eV.

Code	$T = 500$ eV	$T = 1000$ eV
CASSANDRA	12.25	12.87
CORONA	12.14	12.80
OPAL	12.31	12.88
THERMOS	12.28	12.88
ATMED	12.26	12.88
LEDCOP	12.33	12.88
OPAQS	12.31	12.88

The degree of ionization helps in analyzing the overall behavior of plasma at various plasma conditions. We have tested the effect of rise in temperature on the ionization state of plasma. The computation is performed for iron plasma at three different densities of 0.001 g/cc, 0.01 g/cc, and 0.1 g/cc. The results are shown in Fig. 3. It is observed that to attain the same ionization degree, higher temperatures are required at high densities. The shell effect is clearly seen at all densities.

Table 2. Comparison of average charge state for germanium plasma computed at density of 0.01 g/cc and temperatures of $T = 300$ eV and $T = 500$ eV.

Code	$T = 300$ eV	$T = 500$ eV
CASSANDRA	26.60	29.74
CORONA	26.90	29.83
OPAL	26.71	29.82
THERMOS	26.79	29.82
ATMED	26.77	29.82
OPAQS	26.86	29.82

Table 3. Comparison of average charge state for iron plasma computed at different densities and temperatures.

ρ_m/(g/cc)	1		0.0127	7.86
T/eV	500	1000	59	200
CASSANDRA	22.32	23.91	12.49	14.68
CORONA	21.96	23.67	12.93	13.22
OPAL	22.53	23.86	12.79	13.37
THERMOS	22.35	23.91	12.79	14.13
ATMED	22.29	23.87	12.94	14.17
LEDCOP	22.68	23.94	12.83	14.42
OPAQS	22.41	23.97	12.89	14.42

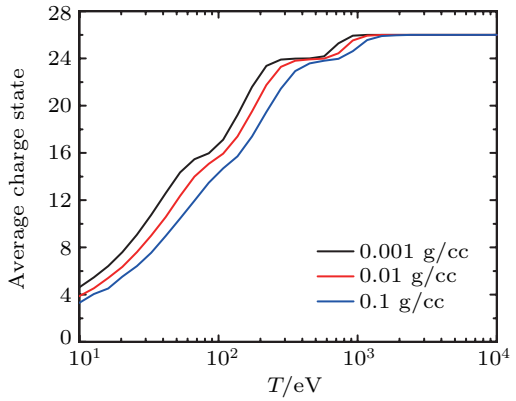


Fig. 3. (color online) Average ionization of iron plasma versus temperature at densities of 0.001 g/cc, 0.01 g/cc, and 0.1 g/cc.

After verifying that the atomic model of OPAQS gives a correct degree of ionization, we proceed to test its calculations for radiative properties. The different contributions to opacity as a function of frequency are shown in Fig. 4 for iron plasma at $\rho_m = 1$ g/cc and $T = 500$ eV. Thomson scattering is included in all cases. The graphical trends show the behaviors of continuum opacity (bound–free + free–free + scattering) as well as total frequency-dependent opacity. The effect of eliminating the contributions of the bound–bound and bound–free transitions is also checked. It is clear that in the

low photon energy range < 0.2 keV, the main contribution to opacity is from inverse bremsstrahlung (FF). In photon energy range ~ 0.2–220 keV, the dominant mechanisms of absorption in determining the total opacity are photo-ionization (BF) and line absorption (BB). Photo-ionization edges accompanied by peaks show that various excitations are taking place along with the ionizations. At 220 keV, almost all the atoms have become fully ionized, so contributions of all the three major phenomena, bound–bound, bound–free, and free–free, cease and the only contribution left is that of Thomson scattering (Scatt), which does not depend upon the frequency. Hence, further increase in photon energy does not change the opacity anymore and we obtain a limiting value of opacity corresponding to scattering only. It is evident that plasma is almost transparent to the high-energy photons, except the minute attenuation caused by scattering.

For opacity validation, a graphical comparison between OPAQS and LEDCOP is presented in Fig. 5 for iron at density of 1 g/cc and different temperatures. It is observed that the opacity trends of OPAQS match very well with those of LEDCOP. The maxima of bound–bound transitions lie at the same energy in both cases. Finding these classical trends gives an indication of the correct implementation of the equations in the code. However, our results have few discrepancies. There is difference in the widths and heights of peaks, which could be due to choice of different line broadening mechanisms. Moreover, OPAQS has lesser number of peaks due to the fact that it is based on average atom approximation whereas LEDCOP utilizes detailed configuration approach. The small discrepancy in the bound–free part in the low-photon energy range is due to merging of photo-ionization edges with the excitation peaks.

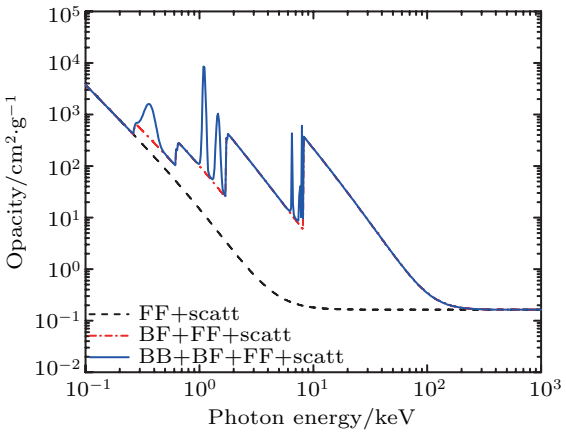


Fig. 4. (color online) Opacity for iron plasma at density of 1 g/cc and temperature of 500 eV. The solid line represents the total frequency-dependent opacity, the dashed-dotted line shows the combined behavior of bound–free, free–free, and scattering terms, and the dashed line shows the effect of combining free–free and scattering contributions.

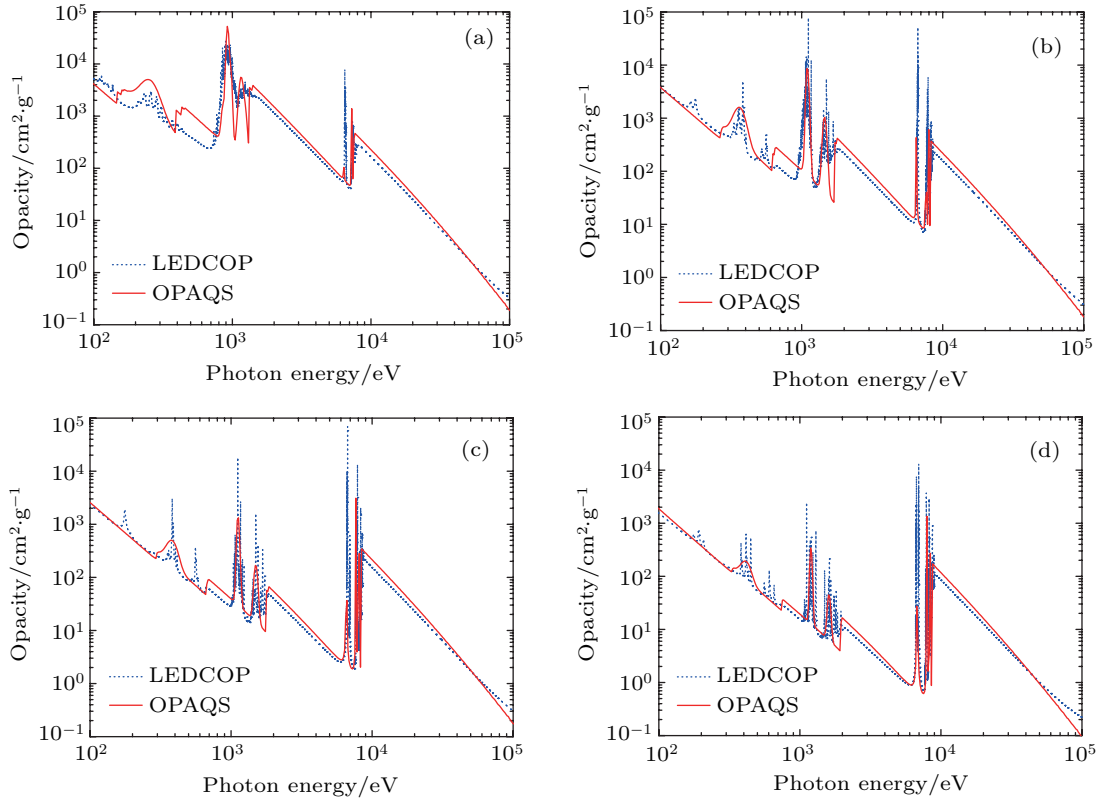


Fig. 5. (color online) Frequency dependent opacities computed with LEDCOP and OPAQS for an iron plasma at density of 1 g/cc and different temperatures: (a) 250 eV, (b) 500 eV, (c) 800 eV, (d) 1250 eV.

Once the behavior of the frequency dependent opacity is tested, the next step is to validate its average behavior, i.e., the Rosseland and Planck mean opacities. The validation of the mean opacities is necessary as they serve as input parameters in radiation transfer computations. We have calculated the mean opacities for the same conditions of iron plasma and presented them in Table 4. For better comparison of atomic models, the values of the average charge state are also tabulated. The results of ATMED code are taken from Ref. [47]. Table 4 shows that the opacities computed with OPAQS are slightly higher than the others, which could be due to broader lines in its opacity trends. The reason is that opacity is mainly contributed by the lines in the absorption spectrum and broader lines tend to close opacity windows, hence increasing the resulting opacity.[21] It is also clear that the higher the temperature, the better the agreement between the obtained opacities. However, at low temperatures, OPAQS is predicting higher values, which is due to the use of the average atom approximation that serves well in the high-temperature region but appears to be slightly crude at low temperatures.[5,6] The atomic model of OPAQS is also limited in describing the energy levels compared to the models employing detailed level approach. In addition, the OPAQS model has omitted relativistic effects, LS splitting, and configuration interaction, whereas these are included in the model of LEDCOP and cause a difference in the atomic data employed in the opacity calculations.[55]

Table 4. Comparison of Rosseland, Planck mean opacities and average charge state for iron at density of 1 g/cc and different temperatures.

T/eV		250	500	800	1250
Rosseland	LEDCOP	908.3	74.97	7.12	2.14
opacity	ATMED	1063.6	62.88	6.32	1.79
/(cm^2/g)	OPAQS	1048.10	83.87	8.36	2.31
Planck	LEDCOP	2745.0	306.50	46.51	30.69
opacity	ATMED	3223.9	348.49	64.78	62.86
/(cm^2/g)	OPAQS	3473.98	364.44	40.61	26.59
	LEDCOP	17.71	22.58	23.49	24.65
Z_o	ATMED	17.83	23.07	23.83	24.80
	OPAQS	17.98	22.79	23.73	24.80

Despite the good comparison of average charge state, OPAQS gives slightly higher values of opacities than those with detailed models, which is also reported elsewhere.[56] The maximum difference in Rosseland mean opacity calculation is found to be 17% at 800 eV, for Planck opacity it is 25% at 250 eV, whereas the maximum deviation in average charge state is 1.5% at 250 eV. In the literature, even the sophisticated codes have reported differences up to 300% in monochromatic opacities[36,57] and up to 60% in Rosseland mean opacities.[58] The reason for these deviations can be justified as follows. The Rosseland mean is a harmonic mean and it depends upon many factors such as features of spectrum (photo-ionization edges, line shapes, and valleys among peaks), numerical methods used in averaging, the grid points, etc. So to get an exact match among the codes or with the experimental data is indeed a challenging task for the theoretical researchers.

In Tables 5 and 6, we have presented the results of Rosseland mean opacity for aluminium and iron at density of 1 g/cc and different plasma temperatures consecutively. For aluminium plasma, the results show very good agreement with the experimental measurements (within the error bound) at temperatures of 750 eV, 1000 eV, and 1250 eV. The only exception is found at temperature of 500 eV where OPAQS is predicting a lower value. It is quite encouraging that OPAQS is in better agreement with the experiment than the rest of the codes. In contrast, the results of iron plasma show good agreement with the experimental data at temperature of 500 eV, whereas at the other three temperatures the values are slightly overestimated, yet still lie in the range predicted by the other codes.

Table 5. Rosseland mean opacity computed for aluminium plasma at density of 1 g/cc and different temperatures. Values are taken from Ref. [47] for comparison.

T/eV	500	750	1000	1250
TF	40.5	9.09	2.09	0.83
OPAL	59.3		2.13	
HOPE	53.1		1.92	
THERMOS	46.1	10.3	2.14	0.83
ATMED	45.02	10.32	2.23	0.85
LEDCOP	56.84		2.19	0.81
OPAQS	30.75	10.61	2.55	0.95
Experiment	51±8	13±2	2.9±0.4	1.1±0.2

Table 6. Rosseland mean opacity computed for iron plasma at 1 g/cc density and different temperatures. Values are taken from Ref. [47] for comparison.

T/eV	500	750	1000	1250
TF	62.5	7.81	2.70	1.59
OPAL	84.2		3.48	
THERMOS	79.60	8.37	3.14	2.29
ATMED	86.16	8.59	2.77	1.77
LEDCOP	74.97		3.32	2.14
OPAQS	83.84	11.03	3.86	2.31
Experiment	82±12	7.8±1.0	2.3±0.4	1.3±0.2

We have also compared the calculations of mean opacities with some other state-of-the-art opacity codes being frequently used in the field of stellar physics: STA, OP, CASSANDRA, OPAS, SCO-RCG, and LEDCOP.[59] Comparison is shown in Table 7. The results of OPAQS are tested by employing two different approaches for the broadening phenomena: Stark broadening is included in the calculations of OPAQS1, but omitted in the case study of OPAQS2. It is observed that OPAQS1 has provided good comparison of Planck

mean opacities with all the other codes, whereas it has discrepancy in the calculation of Rosseland mean values, where all the results are underestimated. The values of Rosseland mean are found to improve when we reduce the effect of Stark broadening in our calculations, but in this way the values of Planck mean opacities get underestimated. The effect of other parameters is also tested by varying their values, but no other parameter is found to play such a strong role. Hence it is interpreted that the line profile is the most sensitive parameter that should be carefully tackled while performing opacity calculations. The correct choice of line broadening mechanism at given temperatures and densities is a hot topic of research nowadays.

Table 7. Planck and Rosseland mean opacities computed for iron plasma at density of 3.4 mg/cc and different temperatures. Values are taken from Ref. [59] for comparison.

T/eV	Planck mean opacity/(cm^2/g)			Rosseland mean opacity/(cm^2/g)		
	15.3	27.3	38.5	15.3	27.3	38.5
STA	58650	33380	16100	19330	20500	7020
OP	23400	28000	14289	8160	14642	5978
CASSANDRA	56770	31250	16280	27650	20250	7545
OPAS	59441	36438	18156	18906	23323	8854
SCO-RCG	54652	30331	13167	18209	19335	6423
LEDCOP	55533	29263	15573	18578	18790	7359
OPAQS1	54749	25208	14344	4113	2505	1687
OPAQS2	46838	23452	13774	19718	13651	1306

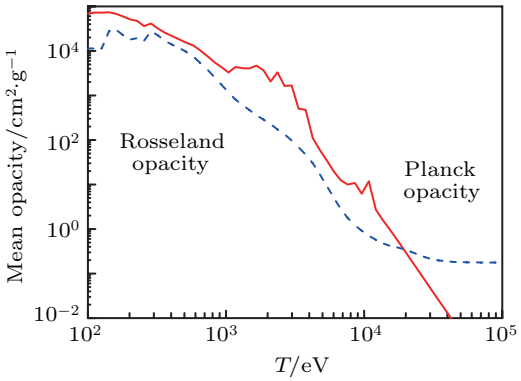


Fig. 6. (color online) Planck and Rosseland mean opacities versus temperature for iron plasma at density of 0.1 g/cc.

We have also tested the temperature dependence of the mean opacities, and the result is shown in Fig. 6. The calculations are performed for iron plasma at density of 0.1 g/cc and a wide range of temperatures. It is clear that both Planck and Rosseland opacities show a decreasing trend. The reason is obvious: with the increase in temperature, the average ionization of plasma increases, which means that now there are fewer number of occupied shells. The lesser number of bound levels results in decreasing the bound–bound and bound–free contributions that strongly need bound electrons for their absorption. The free–free absorption occurs in the field of ions and has very small probability at high temperatures. Thus scattering appears to be the only contributing process. The Planck mean opacity does not include the scattering term so it has a continuously decreasing trend, whereas the Rosseland mean opacity converges to a constant value corresponding to the scattering term that serves as a lower bound in this case. Thus the overall effect of increasing the temperature results in decreasing the opacity.[60] The shell effect is clearly more prominent in the case of Planck mean opacity than that of Rosseland mean opacity.[61]

5. Conclusion

We have developed a new opacity code OPAQS that is based on the average atom model and performs calculations using quantum statistical approach. The code is capable of performing robust calculations of average charge state, frequency-dependent opacities along with grey/mean opacities. The results are compared with available published data on every single step to make sure of the correctness of the calculations. The code is reliable and its frequency-dependent as well as mean opacities show very good agreement with LEDCOP for given plasma conditions. The small discrepancy is due to different approaches employed in both codes.

References

[1] Huebner W F and Barfield W D 2014 *Opacity* (New York: Springer)
[2] Atzeni S and Mayer-ter-vehn J 2004 *The Physics of Inertial Fusion Beam Plasma Interaction, Hydrodynamics, Hot Dense Matter* (Oxford: Oxford University Press)
[3] Gu Y H, Zhao N J, Ma M J, Meng D S, Yu Y, Jia Y, Fang L, Liu J G and Liu W Q 2016 *Chin. Phys. Lett.* **33** 085201
[4] Bailey J E, Rochau G A, Mancini R C, Iglesias C A, MacFarlane J J, Golovkin I E, Blancard C, Cosse P and Faussurier G 2009 *Phys. Plasmas* **16** 058101
[5] Nikiforov A F, Novikov V G and Solomyannaya A D 1996 *High Temp.* **34** 220
[6] Novikov V G, Nikiforov A F and Val'ko V V 1993 *High Temp.* **31** 881
[7] Nikiforov A F, Novikov V G, Uvarov V B and Iacob A 2005 *Quantum-statistical Models of Hot Dense Matter: Methods for Computation Opacity and Equation of State* (Basel: Birkhauser)
[8] Mayer H 1947 *Methods of Opacity Calculations* Los Alamos Scientific Laboratory Report. LA-647. Los Alamos N.M.
[9] More R M 1981 *Atomic Physics in Inertial Confinement Fusion* Lawrence Livermore Laboratory No. UCRL-84991
[10] Rozsnyai B F 1977 *J. Quant. Spectrosc. Radiat. Transfer* **17** 77

[11] Rozsnyai B F 1982 *J. Quant. Spectrosc. Radiat. Transfer* **27** 211
[12] Liberman D A 1982 *J. Quant. Spectrosc. Radiat. Transfer* **27** 335
[13] Tsakiris G D and Eidmann K 1987 *J. Quant. Spectrosc. Radiat. Transfer* **38** 353
[14] Fontes C J, Zhang H L, Abdallah J J, Clark R E H, Kilcrease D P, Colgan J, Cunningham R T, Hakel P, Magee N H and Sherrill M E 2015 *J. Phys. B: At. Mol. Opt. Phys.* **48** 144014
[15] Zeng J and Yuan J 2007 *Phys. Rev. E* **76** 026401
[16] Hu S X, Collins L A, Goncharov V N, Boehly T R, Epstein R, McCrory R L and Skupsky S 2014 *Phys. Rev. E* **90** 033111
[17] Piron R and Blenski T 2011 *High Energy Density Phys.* **7** 346
[18] Zeldovich Y B and Raizer Y P 1966 *Physics of Shock Waves and High Temperature Hydrodynamic Phenomena* (New York: Academic Press)
[19] Rickert A 1995 *J. Quant. Spectrosc. Radiat. Transfer* **54** 325
[20] Serduke F J D, Minguez E, Davidson S J and Iglesias C A 2000 *J. Quant. Spectrosc. Radiat. Transfer* **65** 527
[21] Bailey J E, Nagayama T, Loisel P, Rochau G A, Blancard C, Colgan J, Cosse P, Faussurier G, Fontes C J, Gilleron F and Golovkin I 2015 *Nature* **517** 56
[22] Mondet G, Blancard C, Cosse P and Faussurier G 2015 *Astrophys. J.* **220** 1
[23] Le Pennec M, Turck-Chieze S, Salmon S, Blancard C, Cosse P, Faussurier G and Mondet G 2015 *Astrophys. J. Lett.* **813** 1
[24] Benita A J, Minguez E, Mendoza M A, Rubiano J G, Florido R, Gil J M, Rodríguez R and Martel P 2015 *High Energy Density Phys.* **14** 18
[25] Sheng Z M, Weng S M, Yu L L, Wang W M, Cui Y Q, Chen M and Zhang J 2015 *Chin. Phys. B* **24** 015201
[26] Huang C W, Song T M, Zhao Y, Zhu T, Shang W L, Xiong G, Zhang J Y, Yang J M and Jiang S E J 2012 *Chin. Phys. Lett.* **29** 095201
[27] Liu F, Shao X P, Xiangli B, Gao Y, Han P L and Wang L 2015 *Chin. Phys. Lett.* **32** 114203
[28] Chen Z Q, Hu D, Liu M H, Xia G Q, Zheng X L, Hu Y L, Ye Q B, Chen M G, Zhu L J and Hu X W 2014 *Chin. Phys. B* **23** 035202
[29] Han X Y, Duan X R, Yang L M, Yu D L, Zhong W L, Fu B Z, Liu Y, Liu Y, Yan L W and Yang Q W 2010 *Chin. Phys. Lett.* **27** 055202
[30] Li Y L, Li J, Dong Q F and Wang M J 2014 *Chin. Phys. B* **23** 063301
[31] Bo Y, Zhao Q, Luo X G, Liu Y, Chen Y X and Liu J W 2016 *Acta Phys. Sin.* **65** 035201 (in Chinese)
[32] Qing B, Zhao Y, Wei M X, Li H, Xiong G, Lv M, Hu Z M, Zhang J Y and Yang J M 2016 *Chin. Phys. Lett.* **33** 035203
[33] Badnell N R, Bautista M A, Butler K, Delahaye F, Mendoza C, Palmeri P, Zeippen C J and Seaton M J 2005 *Mon. Not. R. Astron. Soc.* **360** 458
[34] Rogers F J, Wilson B G and Iglesias C A 1988 *Phys. Rev. A* **38** 5007
[35] Porcherot Q, Pain J, Gilleron F and Blenski T 2011 *High Energy Density Phys.* **7** 234
[36] Blancard C, Cosse P and Faussurier G 2011 *Astrophys. J.* **745** 1
[37] Bar-Shalom A, Oreg J and Goldstein W H 1989 *Phys. Rev. A* **40** 3183
[38] Crowley B J B and Harris J W 2001 *J. Quant. Spectrosc. Radiat. Transfer* **71** 257
[39] Nikishawa T, Takabe H and Mima K 1994 *Corona Code escription. In: Rickert A, editor. Proceedings of the third international opacity workshop and code comparison study.* Max Planck Institut für Quantenoptik
[40] Magee N, Merts A, Keady J and Kilcrease D 1994 *Ledcop Code Description. In: Rickert A, editor. Proceedings of the third international opacity workshop and code comparison study.* Max Planck Institut für Quantenoptik
[41] Rubiano J G, Florido R, Rodriguez R, Gil J M, Martel P and Minguez E 2004 *J. Quant. Spectrosc. Radiat. Transfer* **83** 159
[42] Salvat F, Fernandez-Varea J M and Junior W W 1995 *Comp. Phys. Commun.* **90** 151
[43] Buhring W 1965 *Z. fur. Phys.* **187** 180
[44] Kouser R, Tasneem G, Shehzad M S, Ali A, Rehman S and Nasim M H 2015 *11th International Conference, "Interaction of Radiation with Solids"*, September 23–25, Minsk, Belarus, p. 17
[45] Rehman S, Kouser R, Nazir R T, Manzoor Z, Tasneem G, Jehan N, Nasim M H and Sallahuddin M 2015 *11th International Conference, "Interaction of Radiation with Solids"*, September 23–25, Minsk, Belarus, p. 88
[46] Ramis R and Meyer-ter-Vehn J 1992 *Max Planck Institut für Quantenoptik* **174** p. 40
[47] Mendoza M A, Rubiano J G, Gil J M, Rodriguez R, Florido R, Espinosa G, Martel P and Mínguez E 2014 *J. Quant. Spectrosc. Radiat. Transfer* **140** 81
[48] Rickert A and Meyer-Ter-Vehn J 1990 *Laser Part. Beams* **8** 715
[49] Macfarlane J J 1989 *Comp. Phys. Commun.* **56** 259
[50] Sobelman II 1979 *Atomic Spectra and Radiative Transitions* (Berlin: Springer-Verlag)
[51] Menzel D H and Pekeris C H 1935 *Mon. Not. R. Astron. Soc.* **96** 77
[52] Cox P J and Giuli R T 1968 *Principles of Stellar Structure* Vol. 1 (New York: Gordon and Breach)
[53] Mihalas D 1978 *Atmosphere* (San Francisco: Freeman)
[54] Peterson R R and Moses G A 1983 *Comp. Phys. Commun.* **28** 405
[55] Jin F, Zeng J and Yuan 2003 *J Phys. Rev. E* **68** 066401
[56] Zeng J, Zhao G and Yuan J 2006 *Chin. Phys. Lett.* **3** 660
[57] Nagayama T, Bailey J E, Loisel G, Rochau G A, MacFarlane J J and Golovkin I 2016 *Phys. Rev. E* **93** 023202
[58] Gilles D, Turck-Chieze S, Loisel G, Piau L, Ducret J E, Poirier M, Blenski T, Thais F, Blancard C, Cossé P and Faussurier G 2011 *High Energy Density Phys.* **7** 312
[59] Turck-Chieze S and Gilles D 2013 *EPJ Web of Conferences* **43** 01003
[60] Das M, Srivastava M K and Menon S V G 2012 *J. Quant. Spectrosc. Radiat. Transfer* **143** 286
[61] Zaghloul M R 2007 *Plasma Phys. Control Fusion* **49** 1129